Appl. Phys. B 76, 423–427 (2003)
DOI: 10.1007/s00340-003-1119-5

Applied Physics B
Lasers and Optics

W.X. QUE[1,✉]
X. HU[1]
Q.Y. ZHANG[2]

Germania/ormosil hybrid materials derived at low temperature for photonic applications

[1] School of Materials Engineering, Nanyang Technological University, Singapore 639798
[2] School of Electrical and Electronic Engineering, Nanyang Technological University, Singapore 639798

Received: 5 November 2002/
Revised version: 27 December 2002
Published online: 19 March 2003 •

ABSTRACT We report on germania/organically modified silane (ormosil) hybrid materials produced by the sol–gel technique for photonic applications. Acid-catalyzed solutions of γ-glycidoxypropyltrimethoxysilane mixed with germanium isopropoxide have been used as precursors for the hybrid materials. Planar waveguide films with a thickness of about 2 μm have been prepared by a single spin-coating process and low-temperature heat treatment from these high germanium content hybrid materials. Atomic force microscopy, thermal gravimetric analysis, UV–visible spectroscopy, and Fourier-transform infrared spectroscopy have been used to investigate the optical and structural properties of the films. The results have indicated that a dense, low absorption, and high transparency (in the visible range) waveguide film could be achieved at a low temperature. A strong UV-absorption region at short wavelengths ∼ 200 nm, accompanied by a shoulder peaked at ∼ 240 nm, has been noticed due to the neutral oxygen monovacancy defects. The propagation mode and loss properties of the planar waveguide films have also been investigated by using a prism-coupling technique.

PACS 81.05.Pj; 81.20.Fw; 78.66.Sq

1 Introduction

Over the past few years, sol–gel techniques have been playing a significant role towards the development of optical materials in the planar waveguide film format for use in integrated optics [1–4]. This technique possesses a number of advantages over conventional film-formation techniques including a relatively low processing temperature and a good control of the composition and property of the final material. We are aware of the fact that germanosilicate glasses are widely used as the core materials for the production of optical fibers because of their high optical transmission in the visible and infrared range. Especially, they are potentially ideal applications for integrated optics devices, provided that they can be made compatible with single-mode fibers. The use of germania as the core dopant and silica as the substrate ensure that these waveguides will have virtually identical characteristics to single-mode fibers. Moreover, the ultraviolet photosensitivity of germanosilicate glasses has attracted a great deal of attention because of the formation of Bragg gratings and second-harmonic generation [5–7]. These properties provide a significant potential for photonic applications such as data storage, information processing, optical interconnects, and integrated optics. Due to such promising applications, a number of research groups have reported progress in such material systems [8–11]. On the other hand, organically modified silanes (ormosils) have attracted a great attention for integrated optics applications in recent years [12–15], since Schmidt proposed this new type of organic–inorganic hybrids in 1985 [16]. Especially, sol–gel integrated optics of ormosils is beginning to show potential photonic applications and it stimulates studies on optical waveguide materials. Considering that ormosil films of the required thickness of a few microns can be deposited in a single spin-coating process, the moderate processing temperatures could enable direct integration with semiconductor sources and detectors. For example, low-loss waveguides based on titania–ormosil and zirconia–ormosil composite waveguides have been fabricated and studied by the sol–gel technique [17–20]. However, the preparation and properties of germania/ormosil composite waveguide films have not been reported so far. In this paper, we report our recent study on the preparation, characterization, and optical properties of the germania/ormosil hybrid materials for photonic applications. The propagation mode and loss properties of the hybrid planar waveguide films have also been investigated based on a prism-coupling technique.

2 Experiment

2.1 *Sample preparation*

Because of the extreme moisture sensitivity of the germanium alkoxides, all reactions and manipulations were carried out under dry-nitrogen environment. In the preparation of a germania/ormosil hybrid material sol, γ-glycidoxypropyltrimethoxysilane (GLYMO, $(CH_2OCH)CH_2O(CH_2)_3Si(OCH_3)_3$) was used as ormosil source, 1 mole of GLYMO was mixed with 4 moles of ethanol and 4 moles of de-ionized water, and after being stirred for about 30 min, 0.01 mole hydrochloric acid (HCl, 37 wt. % in water) was added to the solution. Then the solution was stirred

✉ Fax: +65-67909081, E-mail: ewxque@ntu.edu.sg

for an hour. Germanium isopropoxide ($Ge[OCH(CH_3)_2]_4$) was added to 2-methoxyethanol ($CH_3OCH_2CH_2OH$) at a molar ratio of 1 : 4 under a nitrogen environment and the solution was agitated until homogenization was reached. Then, the two solutions were mixed with a molar ratio dependent on the desired germanium content in the final sol–gel film. In the present study, the molar ratio of GLYMO to GeO_2 was 4 : 1. The final mixture was stirred for about 25 h at room temperature. Following the common practice for spin coating, a 0.1-micron-pore filter was attached to a syringe for removing foreign particles before the resultant solution was spin-coated onto a substrate. The substrates used in our experiment included silica-on-silicon (SOS) and quartz. One layer of the sol–gel film was spun onto the substrate at 3500 rpm for 30 s. The film-coated samples were then heated for 10 min at different temperatures of 100, 200, 300, 400, and 500 °C.

2.2 *Film characterization*

The hybrid waveguide films (or powders) were characterized by atomic force microscopy (AFM), thermal gravimetric analysis (TGA), UV–visible spectroscopy (UV–VIS), and Fourier-transform infrared spectroscopy (FTIR). The morphology of the films was observed by a Digital Instruments Nanoscope IIIa AFM using the tapping mode. A Perkin-Elmer 7 Series was used for TGA measurement of the gel powders obtained from the corresponding solution, which was done at a heating rate of 5 °C/min in a flowing nitrogen gas environment. The UV–visible absorption spectra were measured for the films deposited on quartz in the range of 200–800 nm on a UV–VIS spectrometer, which has a resolution of ±0.3 nm. The FTIR spectra of the films deposited on silica-on-silicon substrates were measured in the range of 4000–400 cm^{-1} with a resolution of ±1 cm^{-1}.

The refractive index and thickness of the hybrid waveguide films were measured for transverse electric (TE) and transverse magnetic (TM) polarizations by an m-line apparatus (Metricon 2010) based on the prism-coupling technique at the wavelength of 633 nm. The propagation loss was measured by recording the light intensity scattered out of the waveguide plane, which is proportional to the guided intensity. This intensity was recorded by a fiber probe scanning down the length of the propagating streak. The losses were evaluated by fitting the intensity to an exponential decay function, assuming a homogeneous distribution of the scattering centers in the waveguide. The measurements were performed by exciting the transverse electric TE_0 mode of the waveguide with lasers at the wavelengths of 633 and 1550 nm.

3 Results and discussion

The dependence of the morphology of the hybrid films on the heat-treatment temperature has been investigated by AFM. Our results show that dense, nonporous, and smooth film morphology could be obtained at the temperature of below 300 °C. When organic groups are integrated into the inorganic system, the shrinkage of the film is low, perhaps because the bulky organic components fill the pores between the inorganic oxide chains. The film can thus be made to reach its final density at a low temperature. The value of the root mean square (RMS) surface roughness of the films was examined over a 1 μm × 1 μm area. The surface roughness of the film obtained under the present processing condition is sufficiently small for photonics applications. For example, the surface roughness of the film baked at 100 °C is around 0.2 nm (obtained from the 1 μm × 1 μm area). It is also noted that, with an increased temperature, the RMS roughness becomes slightly reduced and thus the film becomes relatively smooth.

Figure 1 shows the TGA curves of the gel powder. It can be seen from Fig. 1 that the weight loss occurs at three stages mainly, namely, below 100 °C, between 350 and 450 °C, and between 450 and 550 °C. Below 100 °C, the weight loss is considered to be due to the evaporation of water and the volatilization and thermal decomposition of the remnants of organic solvents. Between 350 and 450 °C, the weight loss is attributed to the carbonization or the combustion of organic compounds, that is to say, this weight reduction is due to the loss of carbon, hydrogen, and oxygen. Between 450 and 550 °C, the weight loss is probably ascribed to the evaporation of physically absorbed water and the further combustion of organic compounds. As there is no major weight loss afterwards, it can be considered that, for the powder sample, the organic groups have been completely burnt off and the sample is inorganic glass. It can be seen clearly from Fig. 1 that the obvious and faster weight loss occurs at the stage between 350 and 450 °C. Obviously, these results are helpful to understand the results obtained by AFM, where the RMS roughness of the film is found to be reduced with the increase of the heat-treatment temperature. When the heat-treatment temperature is increased, the volatilization and thermal decomposition of the organic solvents or the combustion of organic compounds occurs, and the film becomes relatively smooth. It should be mentioned that the microstructure of the powders can be quite different from that of a film; this analysis can, nevertheless, serve as a guide to what might similarly happen to films.

Figure 2 shows the optical absorption spectra of the films heated at different temperatures, these films having been coated on quartz substrates. It is quite clear that the absorbance of the films is relatively low when the heat-treatment temperatures are at 100 and 200 °C. As the heat-treatment temperature is increased to 400 °C, there is a significantly

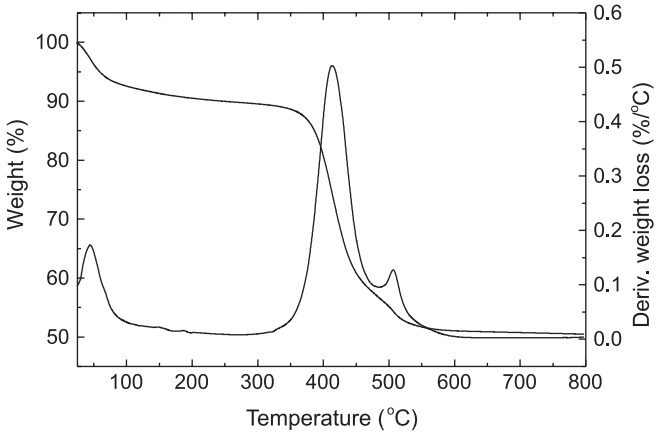

FIGURE 1 TGA curve of gel powder obtained from the solution

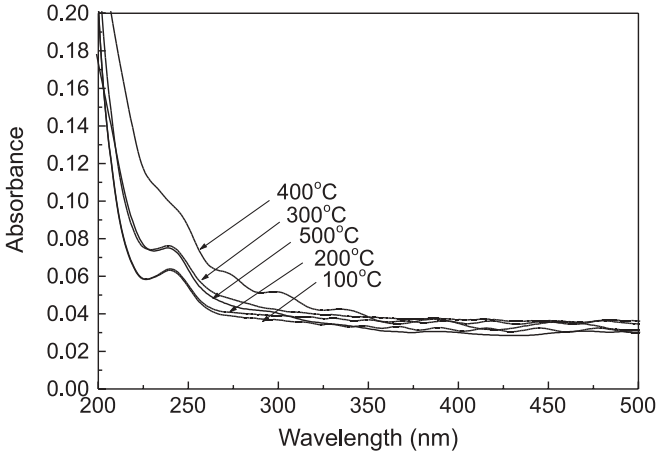

FIGURE 2 UV–VIS absorption spectra of the hybrid films heated at different temperatures

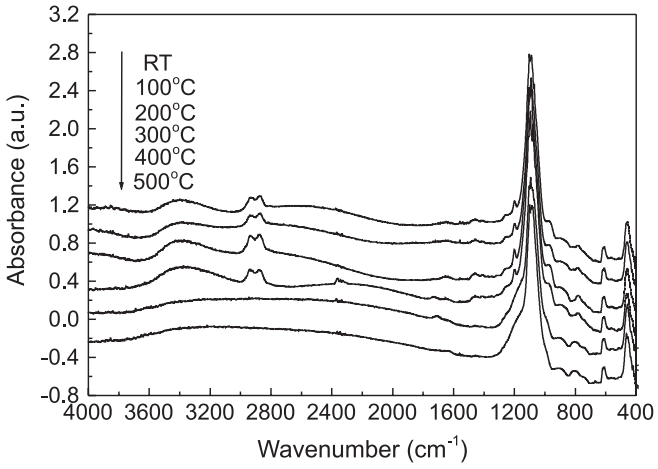

FIGURE 3 FTIR absorption spectra of the hybrid films heated at different temperatures

larger absorption up to 350 nm that can be observed clearly. However, the film heated at 500 °C has a much lower absorbance than that heated at 400 °C, even lower than the film heated at 300 °C. Based on the results obtained by TGA as mentioned before, this behavior could be explained as follows. The film heated at 400 °C was porous due to the incomplete decomposition of the organic compounds. As a result, a relatively large degree of scattering of incident light could also occur by the pores caused by the incomplete decomposition and combination of the organic compounds. When the heat-treatment temperature was increased to 500 °C, the organic compounds have been nearly decomposed and a relatively dense film was obtained. As a result, both the absorption and the scattering caused by the relatively large pores are substantially suppressed. It should be mentioned that a strong UV absorption at short wavelengths ~ 200 nm accompanied with an obvious shoulder located at ~ 240 nm is identified. There is a consensus over the assignment of the absorption band at around ~ 200 nm to Si E′ and Ge E′ centers [21–23]. The absorption at ~ 240 nm is also well characterized and associated with an increase in the concentration of neutral oxygen monovacancy defects [21–25]. It can be seen clearly from Fig. 2 that a decrease in the ~ 240-nm absorption is observed when the heat-treatment temperature increases, because of the reduction of the neutral oxygen monovacancy defects. For the film heated at 400 °C, there is no obvious ~ 240-nm absorption band observed. An explanation is that the large degree of scattering of incident light by the pores caused by the incomplete decomposition and combination of the organic compounds covers the ~ 240-nm absorption band. It can be concluded from the UV-absorption results that a heat-treatment temperature below 300 °C is necessary to attain a dense, low absorption, and high transparency (in the visible range) sol–gel hybrid waveguide thin film by the present process. A decrease of the ~ 240-nm absorption can be observed when the heat-treatment temperature increases from room temperature to 500 °C, because of the reduction of the neutral oxygen monovacancy defects.

The structural properties of the as-deposited and the treated films were studied by FTIR. Figure 3 shows the FTIR spectra of the films heated at different temperatures. The main band peak at 1092 cm^{-1} is assigned to Si−O−R stretching vibrations of ethoxy groups directly bonded to silicon [26]. This band decreases in intensity with increased heat-treatment temperature. A simple explanation is that the reduction of the silicon content may weaken Si−O stretching. There are two weak peaks at 1195 cm^{-1} and 1260 cm^{-1} which correspond to $-CH_3$ rocking vibration from Si−O−CH_3 functional groups and the vibration of the Si−C bond [27], respectively, but these peaks vanish when the heat-treatment temperature is increased to 400 °C or above. The band at 965 cm^{-1}, which is present in those samples heated below 400 °C, is attributed to Ge−O−Ge anti-symmetric stretching. We also observe that the broad peak centered at 2892 cm^{-1} is assigned to $-CH_2-$ symmetric stretching. Furthermore, a broad band between 3100 cm^{-1} and 3600 cm^{-1} is attributed to O−H stretching vibration. It should be noted that a broad OH stretching vibration and a $-CH_2-$ symmetric stretching vibration would not be found with a heat treatment at the temperature up to 400 °C or above. In short, an increase in the heat-treatment temperature leads to a decrease or even the vanishing of the hydroxyl content. It should be mentioned that the peaks at 600 and 460 cm^{-1} observed for all the samples are from the substrate.

The optical waveguide properties of the films were studied using an m-line apparatus based on the prism-coupling technique [28]. The theory of prism coupling has been treated extensively. In its simplest form, the coupler makes use of a high-refractive-index prism placed in close proximity to the planar waveguide. In order to excite all possible waveguide modes, the phase-matching condition between prism and film needs to be met. This requires the refractive index of the prism to be larger than that of the film. By using the prism-coupling technique, light-wave guiding was easily demonstrated in our hybrid films. In order to further characterize the waveguide properties of the films, such films were deposited on silica-on-silicon substrates to fabricate planar waveguides and to observe the propagation mode of light-wave guiding. A laser beam is coupled into the film through a prism. The effective mode index (N_m) is calculated as [29]

$$N_m = N_p \sin\left(\sin^{-1}(\sin\theta_m/N_p) + A_p\right) \quad (1)$$

where N_p is the refractive index of the prism, A_p is its base angle, and θ_m is the incident angle of the laser beam to the prism. In our case, $N_p = 2.1653$ at 633 nm and 2.1227 at 1550 nm, and $A_p = 50.75°$.

The film heated at 200 °C was found to support several TE modes or TM modes at 633 nm, as shown in Fig. 4a and b, respectively. However, considering that the substrate index is about 1.457 for a wavelength of 633 nm, only the two highest indices for each polarization are higher than this value, that is to say, only two modes of TE_0 and TE_1 (TM_0 and TM_1) can be guided modes of the waveguide and used for calculating the profile parameters. The incident mode angles, θ_m, and the calculated effective mode indices, N_m, for the TE_0, TE_1, TM_0, and TM_1 modes are listed in Table 1. From theory [30], the refractive index and the thickness of the film can be determined from the measured effective refractive index values of both TE and TM modes. For TE modes, the results obtained are 1.5081 and 1.95 μm, while for TM modes, they are 1.5085 and 1.97 μm, respectively. It is quite encouraging to note that the values obtained from the TE and TM modes are in good agreement. The small difference of the refractive indices obtained for TE and TM modes indicates that the birefringence in the waveguide is negligible. Figure 5 shows the dependence of the thickness and refractive index of the films on the heat-treatment temperature from 50 to 300 °C. As expected, with the heat-treatment temperature increase, the refractive index of the film increases and the thickness drops. It can be also seen from Fig. 5 that the film thickness and refractive index are not sensitive to an increase of the heat-treatment temperature from 50 to 200 °C. For example, the decrease of the film thickness is about 1% and the increase of the refractive index is about 0.03%, respectively, when the heat-treatment temperature is increased from 100 to 200 °C. However, the change in the film thickness and refractive index is more substantial when the temperature is between 200 and 300 °C. It can be concluded that a dense and nonporous hybrid waveguide film can be obtained below the heat-treatment temperature of 300 °C. With the further increase of the heat-treatment temperature, the thermal decomposition of the organic solvents or the combustion of the organic compounds occurs and the film becomes an inorganic film.

The optical propagation losses at 633 nm and 1550 nm, for the TE_0 mode, were evaluated by a scattered-light measurement technique based on a fiber photometric detection. The losses were typically 7.3 dB/cm at 633 nm and 2.4 dB/cm at 1550 nm for the waveguide film heated at 100 °C. It is obvious that the loss of the waveguides prepared at the present process conditions is relatively large as compared to those reported previously for a SiO_2-GeO_2 planar waveguide [8, 31]. The total loss of a planar waveguide consists of absorption and scattering contributions, the latter being usually predominant at the wavelength of interest in integrated optics. The scattering loss for an amorphous waveguide is the sum of two contributions, including surface scattering due to the surface roughness of the film, and volume scattering due to local fluctuations in the refractive index resulting from density and compositional variations [19]. Actually, the measured wave-

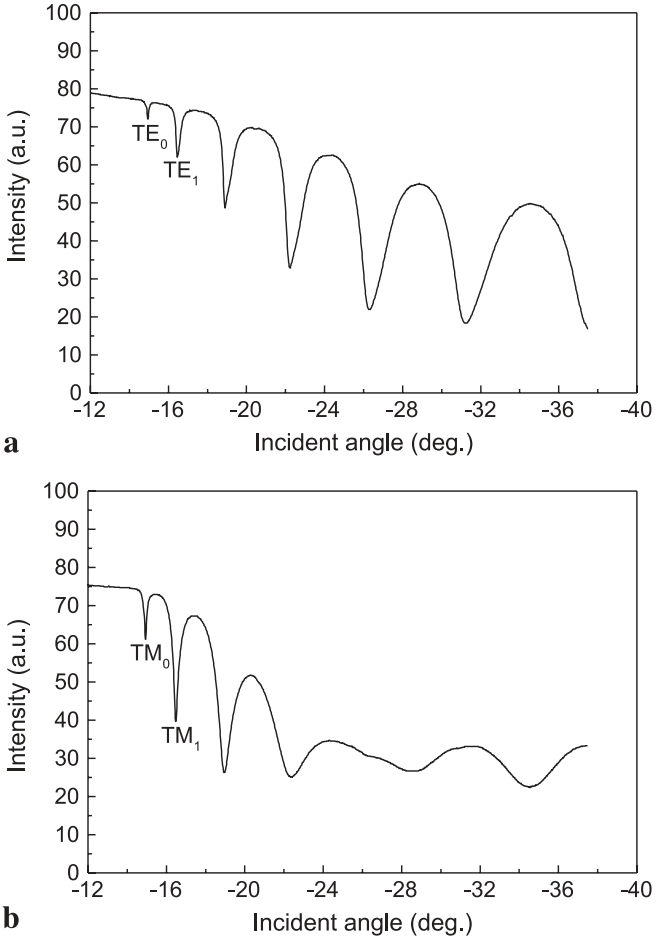

FIGURE 4 Optical guided modes of the hybrid waveguide film at the wavelength of 633 nm. **a** TE modes, **b** TM modes

Mode	Incident angle	Effective mode index	Film refractive index	Film thickness (μm)
TE_0	−14.94°	1.5017		
TE_1	−16.45°	1.4832	1.5081 (at 633 nm)	1.95
TM_0	−14.94°	1.5017		
TM_1	−16.48°	1.4828	1.5085 (at 633 nm)	1.97

TABLE 1 Incident angle, effective mode index of the guided modes obtained by the m-line technique, and refractive index and film thickness calculated from the effective mode refractive index at 633 nm

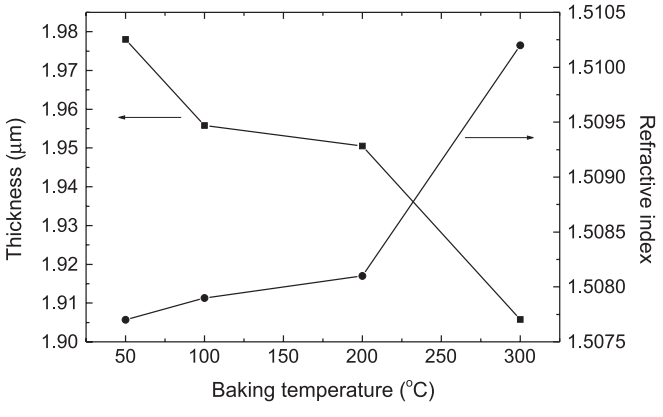

FIGURE 5 Dependence of the thickness and refractive index of the hybrid films on heat-treatment temperature

guide films have several defects, possibly dust, which visibly scattered light to a greater extent than the surrounding sol–gel medium. Loss measured through sections of a film containing these defects should be higher. It is also possible for a guided wave propagating in a planar medium that local refractive index fluctuations in the volume of the guide and deviations from a perfectly plane geometry at the waveguide–cladding boundaries contributed to the losses. In addition, large surface roughness of the film and nonuniform hydrolysis and condensation of the binary alkoxide mixture undoubtedly resulted in the big scattering loss. The homogeneity of a sol–gel glass synthesized from a mixture of two or more alkoxide precursors has been affected by the relative rates of homocondensation and heterocondensation. Silicon alkoxides hydrolyze rather slowly, and acid or base catalysis has been employed frequently for accelerating the reaction quite effectively. However, germanium alkoxides hydrolyze at a much faster rate and, as a result, in mixtures of germanium and silicon alkoxides, it is still possible that a heterogeneous network containing Ge-rich and Si-rich domains is formed in this system [31]. It is strongly expected that a waveguide film with a lower loss can be obtained if the fabrication processing of the waveguide is carried out in a clean-room environment.

4 Conclusions

Germania/ormosil hybrid materials have been studied in an optical planar waveguide configuration for photonic applications. A waveguide thin film with a thickness of about 2.0 μm has been prepared by the sol–gel single spin-coating technique and a low-temperature heat treatment. The effects of the heat-treatment temperature on the structural and optical properties of the waveguide films have been studied by AFM, TGA, UV–VIS, and FTIR spectroscopy. The results indicate that a heat-treatment temperature below 300 °C is expected to produce a dense, low absorption, highly transparent hybrid waveguide film. The introduction of ormosil GLYMO provides the advantage of producing thicker films and obtains a dense film at low temperature. This trend particularly facilitates their use with semiconductor and integrated optical devices. A strong UV-absorption region at short wavelengths ~ 200 nm, accompanied with a shoulder peaked at ~ 240 nm, due to the neutral oxygen monovacancy defects, has been identified. Both propagation mode and loss properties of the waveguide films have been studied by using the prism-coupling technique. About 2.4 dB/cm propagation loss of the planar waveguide film heated at 100 °C has been obtained based on the scattered-light measurement technique at 1550 nm.

REFERENCES

1 M. Benatsou, B. Capoen, M. Bouazaoui, W. Tchana, J.P. Vilcot: Appl. Phys. Lett. **71**, 428 (1997)
2 X. Orignac, D. Barbier, X.M. Du, R.M. Almeida: Appl. Phys. Lett. **69**, 895 (1996)
3 C. Strohhöfer, J. Fick, H.C. Vasconcelos, R.M. Almeida: J. Non-Cryst. Solids **226**, 182 (1998)
4 C. Duverger, M. Ferrari, C. Mazzoleni, M. Montagna, G. Pucker, S. Turrell: J. Non-Cryst. Solids **245**, 129 (1999)
5 H. Shigemura, Y. Kawamoto, J. Nishii, M. Takahashi: J. Appl. Phys. **85**, 3413 (1999)
6 A. Partovi, T. Erdogan, V. Mizrahi, P.J. Lemaire, A.M. Glass, J.W. Fleming: Appl. Phys. Lett. **64**, 821 (1994)
7 T. Fujiwara, M. Takahashi, A.J. Ikushima: Appl. Phys. Lett. **71**, 1032 (1997)
8 D.G. Chen, B.G. Potter, J.H. Simmons: J. Non-Cryst. Solids **178**, 135 (1994)
9 K.D. Simmons, B.G. Potter, Jr., G.I. Stegeman: Appl. Phys. Lett. **64**, 2537 (1994)
10 C. Strohhöfer, S. Capecchi, J. Fick, A. Martucci, G. Brusatin, M. Guglielmi: Thin Solid Films **326**, 99 (1998)
11 S. Grandi, P. Mustarelli, A. Magistris, M. Gallorini, E. Rizzio: J. Non-Cryst. Solids **303**, 208 (2002)
12 D.L. Ou, A.B. Sedon: J. Sol–Gel Sci. Technol. **8**, 139 (1997)
13 M.P. Andrews, S.I. Najafi: Proc. SPIE Crit. Rev. Opt. Sci. Technol. **68**, 253 (1997)
14 Y. Sorek, R. Reisfeld, R. Tenne: Chem. Phys. Lett. **227**, 242 (1994)
15 A. Martucci, P. Innocenzi, J. Fick, J.D. Mackenzie: J. Non-Cryst. Solids **244**, 55 (1999)
16 H. Schmidt: J. Non-Cryst. Solids **73**, 681 (1985)
17 H. Schmidt, H. Krug, R. Kasemann, F. Tiefensee: Proc. SPIE **1590**, 36 (1991)
18 Y. Sorek, R. Reisfeld, A.M. Weiss: Chem. Phys. Lett. **244**, 371 (1995)
19 S.J.L. Ribeiro, Y. Messaddeq, R.R. Goncalves, M. Ferrari, M. Montagna, M.A. Aegerter: Appl. Phys. Lett. **77**, 3502 (2000)
20 W.X. Que, C.H. Kam: Opt. Eng. **41**, 1733 (2002)
21 M.G. Sceat, G.R. Atkins, S.B. Poole: Annu. Rev. Mater. Sci. **23**, 381 (1993)
22 P.J. Hughes, A.P. Knights, B.L. Weiss, S. Kuna, P.G. Coleman, S. Ojha: Appl. Phys. Lett. **74**, 3311 (1999)
23 Y. Miyake, H. Nishikawa, E. Watanabe, D. Ito: J. Non-Cryst. Solids **222**, 266 (1997)
24 H. Hosono, H. Kawazoe, K.I. Muta: Appl. Phys. Lett. **63**, 479 (1993)
25 M. Takahashi, T. Fujiwara, T. Kawachi, A.J. Ikushima: Appl. Phys. Lett. **71**, 993 (1997)
26 L. Smith: Spectrochim. Acta **16**, 87 (1960)
27 N.B. Colthup, L.H. Daly, S.E. Wiberley: *Introduction to Infrared and Raman Spectroscopy* (Academic, New York 1964)
28 R. Syms, J. Cozens: *Optical Guided Waves and Devices* (McGraw-Hill International, London 1992)
29 E. Pelletier, F. Flory, Y. Hu: Appl. Opt. **28**, 2918 (1989)
30 P.K. Tien, R. Ulrich, R.J. Martin: Appl. Phys. Lett. **14**, 291 (1969)
31 L. Yang, S.S. Saavedra, N.R. Armstrong, H. John: Anal. Chem. **66**, 1254 (1994)